Osaka University Knowledge Archive

Title	Solid State Diffusion Bonding of Silicon Nitride with Vanadium Foils(Materials, Metallurgy & Weldability)
Author(s)	Maeda, Masakatsu; Igarashi, Osamu; Shibayanagi, Toshiya et al.
Citation	Transactions of JWRI. 2003, 32(2), p. 291-301
Version Type	VoR
URL	https://doi.org/10.18910/12394
rights	
Note	

Osaka University Knowledge Archive : OUKA

https://ir.library.osaka-u.ac.jp/

Osaka University

Trans. JWRI, Vol.32, (2003), No.2

Solid State Diffusion Bonding of Silicon Nitride with Vanadium Foils†

MAEDA Masakatsu*, IGARASHI Osamu, SHIBAYANAGI Toshiya*** and NAKA Masaaki******

Abstract

This paper describes the relation between the interfacial microstructure and the fracture strength of joints of silicon nitride (Si_3N_4) and vanadium (V) formed by solid state diffusion bonding. At first, the interfacial microstructure and its evolution process were analyzed in detail. The phase sequence at the interface changes with the bonding time showing five typical stages, including a metastable state in the first stage of the interfacial reaction. V_3Si, V_2N, $V_5Si_3N_{1-X}$ and VN are formed. V_2N is formed in contact with V_3Si at 1473 K and below, while the contact is prohibited at 1498 K and above. The evolution process of the interfacial microstructure is successfully described on a chemical potential diagram with continuous and monotonously changing curves, except for the metastable first stage. The growth behaviors of each reaction product interact with each other. The behavior of the V_3Si layer is affected not only by the formation and growth of the $V_5Si_3N_{1-X}$ layer but also by the formation of a V(Si) zone at the V_3Si / V interface. The formation of the $V_5Si_3N_{1-X}$ layer starts when the spatial gradient of the chemical potential of vanadium in the V_3Si layer decreases to -3.3×10^9 J mol^{-1}. The fracture strength of the joints changes depending on the bonding temperature and time. A higher bonding temperature leads to a higher maximum fracture strength. The maximum strength at each bonding temperature is achieved when the thickness of the V_3Si layer is 2.0 μm. A prolonged bonding time gradually reduces the fracture strength down to 42 MPa.

KEY WORDS: (structural ceramics), (solid state diffusion bonding), (interfacial microstructure), (microstructural evolution), (thermodynamics), (reaction kinetics), (joint strength and fracture), (silicon nitride), (vanadium)

1. Introduction

Silicon nitride (Si_3N_4) displays a low density of 3.2 × 10^3 kg m^{-3} retaining high strength and creep resistance at high temperatures, favorable electrical insulation and thermal shock resistance[1, 2]. These properties are suitable for high-temperature structural applications. Advanced fusion generators are one of such high-temperature structures. Fusion generators demand Si_3N_4 to be applied as the insulator coating on vanadium to reduce the magneto-hydrodynamic pressure drop of liquid lithium coolant[3-8]. Since Si_3N_4 exhibits high resistance to radiation damage with low radio-activation characteristics of its constituent elements[2, 5, 9] in addition to the merits listed above. However, it is still difficult to obtain sound joints of Si_3N_4 and metallic materials, which endure the high temperatures at which Si_3N_4 exhibits its merits.

Vanadium and its alloys have become the leading candidate materials for first-wall and blanket structures for fusion generators because of their low radio-activation characteristics and retention of high strength and fracture toughness at high working-temperatures[3-6]. On the other hand, vanadium is known as one of the chemically active additive elements for brazing Si_3N_4[10-12]. This implies that vanadium enhances adsorption and wetting between Si_3N_4 and brazing alloys. However, braze materials which consist mainly of silver, copper or nickel are not preferred for the construction of first-walls, because those elements are severely radio-activated. Thus, direct bonding of Si_3N_4 and vanadium is required. Unfortunately, very few reports concern the direct diffusion bonding of Si_3N_4 and vanadium[13-16]. Since vanadium is a chemically active element, chemical reactions with Si_3N_4 are expected to occur. Those reports have predicted the production of vanadium silicides and nitrides, showing different analysis results for the interfacial microstructures among them. This implies that the detailed interfacial microstructure of the Si_3N_4 / vanadium joints is still unclear. Furthermore, the

† Received on December 1, 2003

* Research Associate
** Graduate Student
*** Associate Professor
**** Professor

Transactions of JWRI is published by Joining and Welding Research Institute of Osaka University, Ibaraki, Osaka 567-0047, Japan

evolution processes of the interfacial microstructures at elevated temperatures has never been reported. Such basic knowledge on the interfacial microstructure and its formation mechanism is necessary to control the microstructure and the performance of the joints precisely.

The present study aims to describe in detail the interfacial microstructure and its evolution process at elevated temperatures during direct solid state diffusion bonding of Si_3N_4 and vanadium. The proper state of the interfacial microstructure is then deduced on the basis of the relation between the microstructure and the fracture strength.

2. Experimental

Si_3N_4 specimens were prepared from pressureless sintered columnar rods, whose diameter and length were 6.0 mm and 40.0 mm, respectively. They contained a few mass percent each of Al_2O_3, Y_2O_3 and WSi_2 as the sintering agents. The rods were cut to length of 4.0 mm. The surfaces to be joined were polished with 3 μm diamond paste. The roughness of the surface produced was about 0.032 μm. On the other hand, the specimens of vanadium were 25 μm-thick foils with a nominal purity of 99.9 %. Both sides of the vanadium foils were polished with 0.3 μm alumina suspension just before the bonding treatment to remove oxide scale on their surfaces. The surface roughness of the foils was about 0.13 μm.

After cleaning in an ultrasonic acetone bath, a vanadium foil was inserted between two Si_3N_4 specimens. They were set into an induction-heating vacuum furnace, applying uniaxial pressure of 140 MPa perpendicular to the bonding interfaces. The vacuum inside the furnace was kept below 1×10^{-3} Pa. The bonding temperatures and times ranging from 1273 K and 1673 K and from 0.3 ks to 360 ks, respectively, were used.

The interfacial structure of the joints was analyzed by a combination of scanning electron microscopy (SEM), wavelength-dispersive electron probe microanalysis (EPMA) and X-ray diffractometry (XRD). The quantitative composition measurement by EPMA was implemented utilizing a ZAF correction program.

The strength of the joints was evaluated by a shear fracture test, which is adequate for short-sized specimens of 8 mm. The fracture test was implemented with a cross-head speed of 1.67×10^{-5} m s^{-1} at ambient temperature and atmosphere. Five samples at least were tested for each bonding condition. The fractured surfaces were also analyzed by SEM, EPMA and XRD.

3. Results and Discussion

3.1 Bondability

With some combinations of bonding temperature and time, solid state diffusion bonding experiments failed to produce joints of Si_3N_4. The bondability at each employed bonding condition are listed in **Table 1**, in which "S" means that the bonding at the condition succeeds, while "F" means that it fails. In order to obtain sound joints of Si_3N_4 using vanadium inserts, the bonding

Table 1 Success-and-failure diagram of the Si_3N_4 / V / Si_3N_4 bonding experiments.

Bonding time, t / ks	Bonding temperature, T / K				
	1273	1373	1473	1573	1673
0.2				S	S
0.3			F	S	S
0.9	F	F	F	S	S
1.8	F	F	S	S	S
3.6	F	S	S	S	S
14.4	F	S	S	S	S
32.4	S	S	S	S	S
43.2			S		
57.6			S		
90.0			S		
360.0			S		

time of 32.4 ks, 3.6 ks, and 1.8 ks or longer is required for bonding at 1273 K, 1373 K, and 1473 K, respectively. At bonding temperatures of 1573 K and above, very short bonding times of 0.2 ks are enough to obtain sound joints. This result indicates that longer time is required for bonding at lower temperatures. Thus, the formation kinetics of the interfacial microstructure has been investigated in relation to the bonding temperature and time.

3.2 Interfacial Microstructures of Si_3N_4 / V Joints

The interfacial microstructures of Si_3N_4 / V joints bonded at low temperatures of 1273 K, 1373 K and 1473 K appear different from those at high temperatures of 1573 K and 1673 K. The interfacial microstructures at 1473 K and 1673 K are described in the following sections, which reports the structures at low- and high-temperature bonding conditions, respectively.

Fig. 1 shows the interfacial microstructure of a joint bonded at 1473 K for 3.6 ks. Fig. 1(a) is an SEM micrograph of the interface. The dark regions on the left- and the right-side-end of the micrograph are Si_3N_4. The bright particles appearing in the Si_3N_4 are the WSi_2 sintering agents. The bright region in the center is vanadium. Defects such as voids and cracks are scarcely observed at the interface. Two types of reaction products are observed between Si_3N_4 and vanadium. One is formed as a 1.87 μm-thick layer, on which "L" is marked, between Si_3N_4 and vanadium. The boundary between Si_3N_4 and the L-phase remains smooth. The other reaction product is formed as grains, on which "G" is marked, in contact with the vanadium and the layered reaction product. Fig. 1(b) shows the elemental distribution profile along the line from X to Y depicted in Fig. 1(a). The L-phase consists of approximately 80 at% V and 20 at% Si with a very low content of nitrogen. Referring to the V-Si binary phase diagram[17], the composition corresponds to V_3Si. On the other hand, the G-phase consists of approximately 74 at% V and 26 at% N with a very low content of silicon. The V-N binary phase diagram[18]

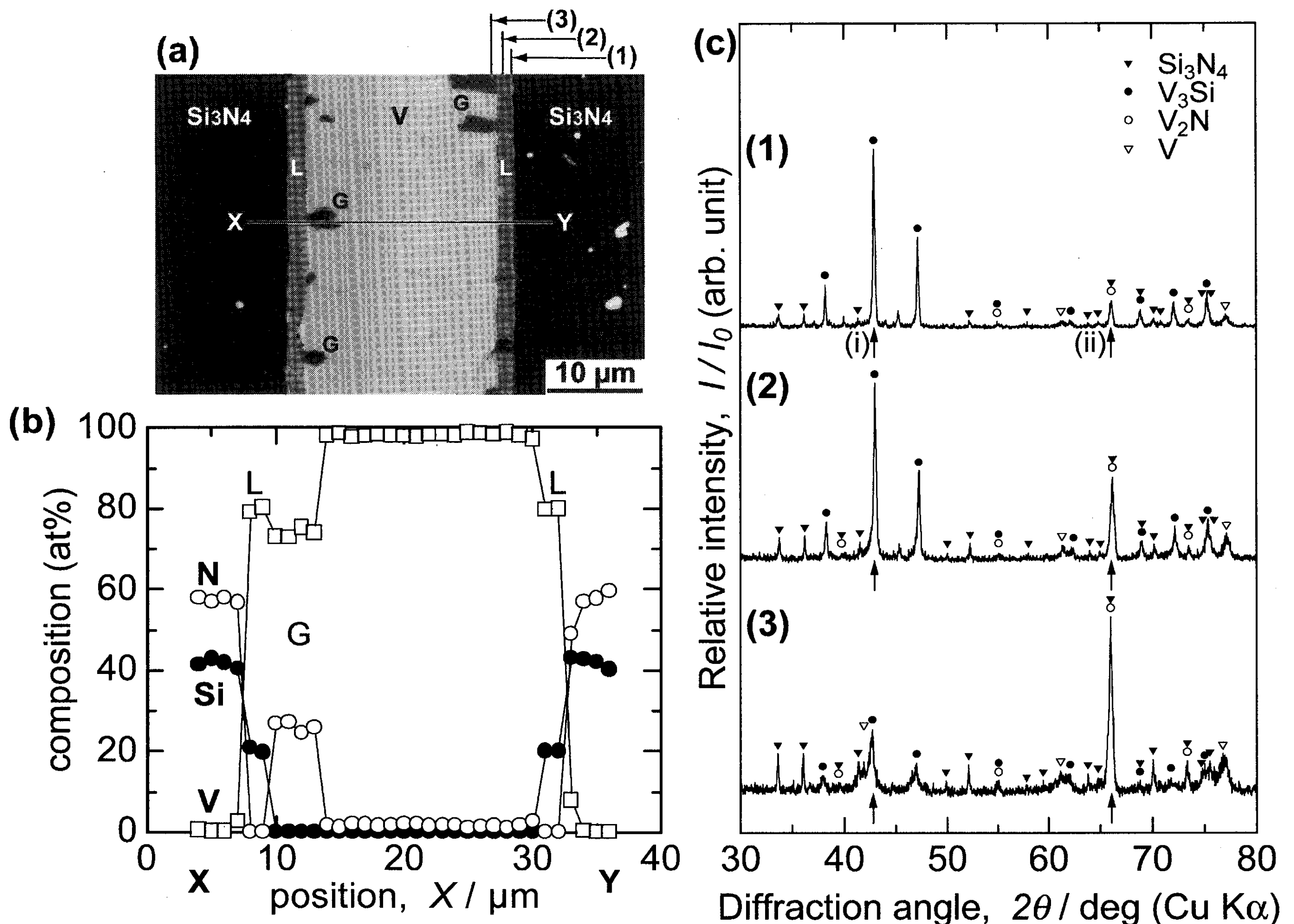

Fig. 1 Interfacial microstructure of the Si_3N_4 / V joint bonded at 1473 K for 3.6 ks. (a) SEM micrograph, (b) composition profile along the line from X to Y depicted in the micrograph, (c) X-ray diffraction patterns from the positions (1), (2) and (3) depicted on the top of the micrograph.

suggests that the composition corresponds to V_2N. Fig. 1(c) shows a series of X-ray diffraction patterns which correspond to the positions (1), (2) and (3) depicted on the top of Fig. 1(a). The specimen was cut at one side of the Si_3N_4 in the vicinity of its interface and ground down carefully about 1 μm for each XRD measurement. Each reaction product and its arrangement were identified by the position of each X-ray diffraction peak and the alteration of its relative intensity. All three patterns in Fig. 1(c) are identified as superimpositions of Si_3N_4[19], V_3Si [20], V_2N[21] and V[22]. The appearance of all existing phases in every XRD pattern is due to the detection depth of the diffracted X-ray and the experimental error in polishing flat and parallel to the interface. However, the alteration of the relative intensity appears clearly in the peaks at 42.83° and 66.13°, which are marked with arrows (i) and (ii), respectively. The peak (i) corresponds only to the 210 plane of V_3Si. Compared with pattern (1), this peak keeps its intensity in pattern (2) and then it is significantly weakened in pattern (3). The peak (ii), on the other hand, corresponds to the 300 plane of V_2N. The relative intensity of the 300 peak of V_2N does not fit the standard diffraction pattern[21] indicating that the 100 plane of V_2N is oriented parallel to the joint interface. Although there is no peak which solely corresponds to V_2N, this orientation of V_2N clearly suggests its existence at the interface by the peak (ii). This peak is intensified in pattern (2) and is more intensified in pattern (3). This result agrees well with the EPMA analysis result depicted in Fig. 1(b). Combining the results of SEM, EPMA and XRD, the L-phase and the G-phase are identified as V_3Si and V_2N, respectively. Therefore, the apparent phase sequence is finally identified as Si_3N_4 / V_3Si / V+V_2N / V.

The interfacial structure of the joints bonded in other conditions of bonding time were also analyzed in the same way. **Fig. 2** shows a series of SEM micrographs, which reveal four typical stages of interfacial microstructures bonded at 1473 K for different bonding times and the result of phase identification. The bonding times for the joints depicted in Figs. 2 (a), (b), (c) and (d) are 3.6 ks, 57.6 ks, 90.0 ks and 360.0 ks, respectively. In the first stage shown in Fig. 2(a), a layer of V_3Si adjacent to Si_3N_4 and grains of V_2N in contact with V_3Si and V are formed. In the second stage shown in Fig. 2(b), $V_5Si_3N_{1-X}$ [14, 23, 24] is formed as a layer between Si_3N_4 and V_3Si. The Si_3N_4 / $V_5Si_3N_{1-X}$ interface becomes rough. The V_2N

grains grow and contact with grains which have grown from the opposite side of the foil. Thus, the phase sequence observed in this stage is described as Si_3N_4 / $V_5Si_3N_{1-X}$ / V_3Si / V+V_2N. In the third stage shown in Fig. 2(c), the V phase is annihilated. The central part of the foil is replaced with V_2N, which has become a layer. The $V_5Si_3N_{1-X}$ layer grows, reducing the V_3Si layer. As the result, the thickness of the V_3Si layer decreases. The $V_5Si_3N_{1-X}$ layer contains large amount of voids, which appear with round-shaped dark contrasts in the micrographs. In particular, large-sized voids are concentrated in the vicinity of the Si_3N_4 / $V_5Si_3N_{1-X}$ interface, as indicated with white arrows in Fig. 2(c). These voids are considered to be N_2 gas phase, which is generated by the decrease of nitrogen solubility in the $V_5Si_3N_{1-X}$ during cooling. Thus, the phase sequence observed in this stage is described as Si_3N_4 / $V_5Si_3N_{1-X}$ / V_3Si / V_2N. In the fourth stage shown in Fig. 2(d), the V_3Si layer is annihilated. Thus, the $V_5Si_3N_{1-X}$ layer contacts with the V_2N layer. At the $V_5Si_3N_{1-X}$ / V_2N interface, VN is newly formed as grains. The phase sequence observed in this stage is described as Si_3N_4 / $V_5Si_3N_{1-X}$ / V_2N + VN / V_2N.

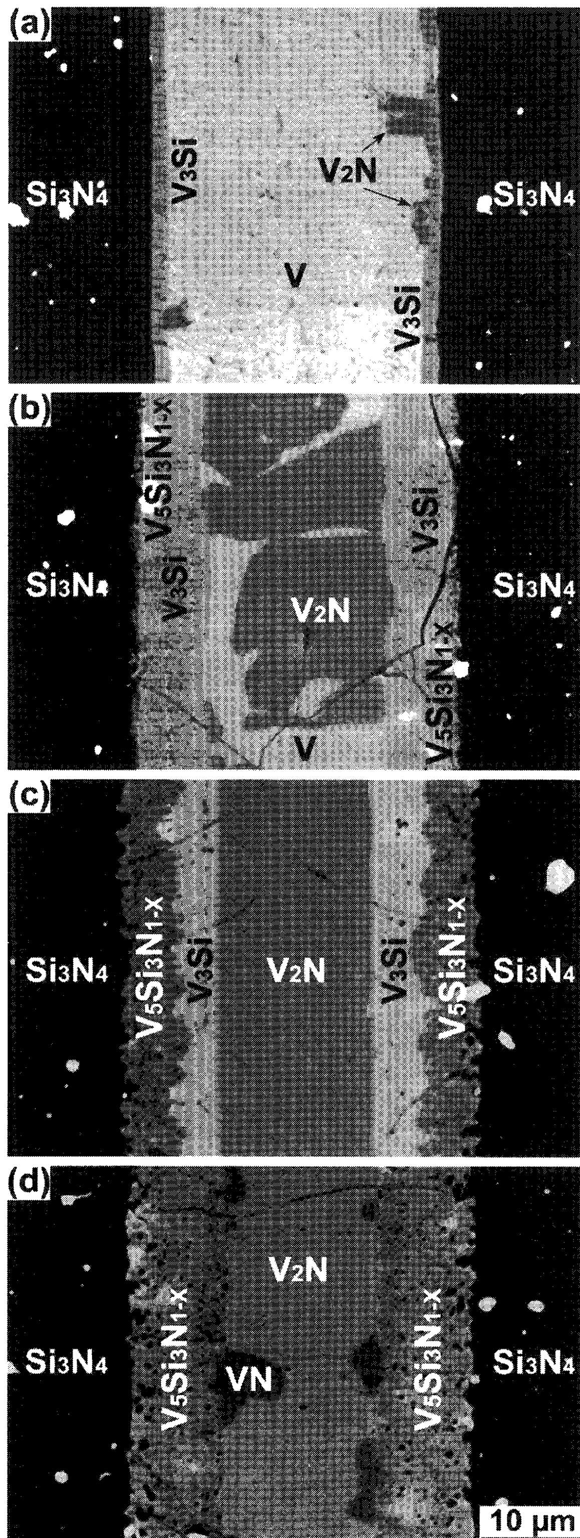

Fig. 2 Four representative stages of the interfacial structure bonded at 1473 K. The bonding time for each joint is (a) 3.6 ks, (b) 57.6 ks, (c) 90.0 ks and (d) 360.0 ks, respectively.

The phase sequence observed at each stage of interfacial structure is confirmed by available V-Si-N ternary phase diagrams[25]. Although the phase diagram presents only two isothermal sections at 1273 K and 1773 K, most of the observed phase sequences are consistent with the isothermal section at 1273 K except in the following two points. One is the Si_3N_4 / V_3Si interface, which is observed in the first stage of the evolution of the

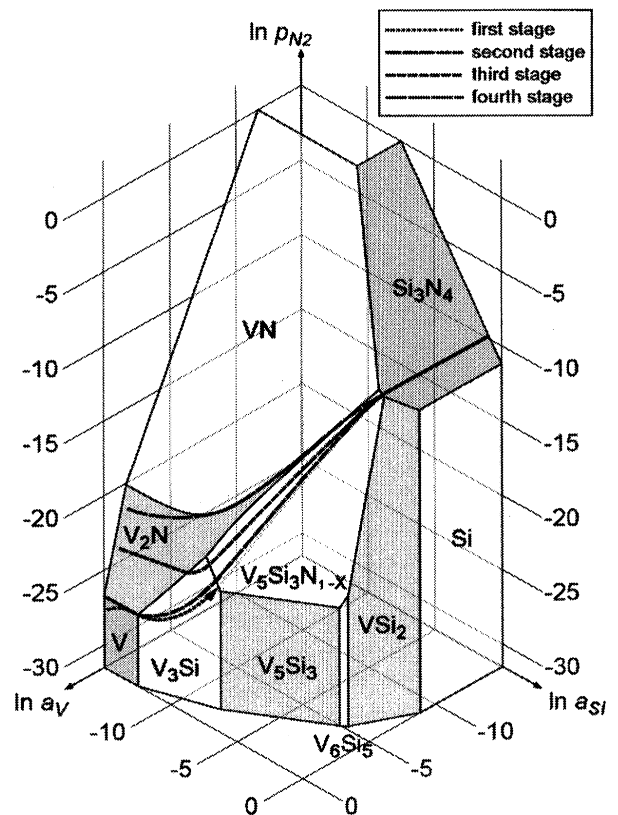

Fig. 3 Chemical potential diagram of the V-Si-N ternary system at 1473 K. The four types of dashed lines depict the phase sequences observed at four different stages of the joint interfaces shown in Fig. 2.

interfacial microstructure. The interface requires a $V_5Si_3N_{1-X}$ layer to exist between Si_3N_4 and V_3Si, which is achieved in the second stage, to equilibrate thermodynamically. Therefore, the Si_3N_4 / V_3Si interface is considered to be in a metastable state, which is observed only in the earliest stage of the interfacial reaction. The other point is the $V_5Si_3N_{1-X}$ / VN interface, which is observed at interfaces in the fourth stage. The thermodynamic state of the $V_5Si_3N_{1-X}$ / VN interface was investigated by considering the chemical states of the constituent elements in each phase, which are calculated from the thermodynamic data[25] and phase diagrams[17, 18, 25]. **Fig. 3** proposes the V-Si-N ternary chemical potential diagram at 1473 K, in which $V_5Si_3N_{1-X}$ is allowed to coexist with VN. This result agrees well with another V-Si-N ternary phase diagram presented by Andruszkiewicz and Horyń[24]. The phase sequences observed in Fig. 2, except the metastable first stage, are compatibly explained by the dashed lines drawn on Fig. 3.

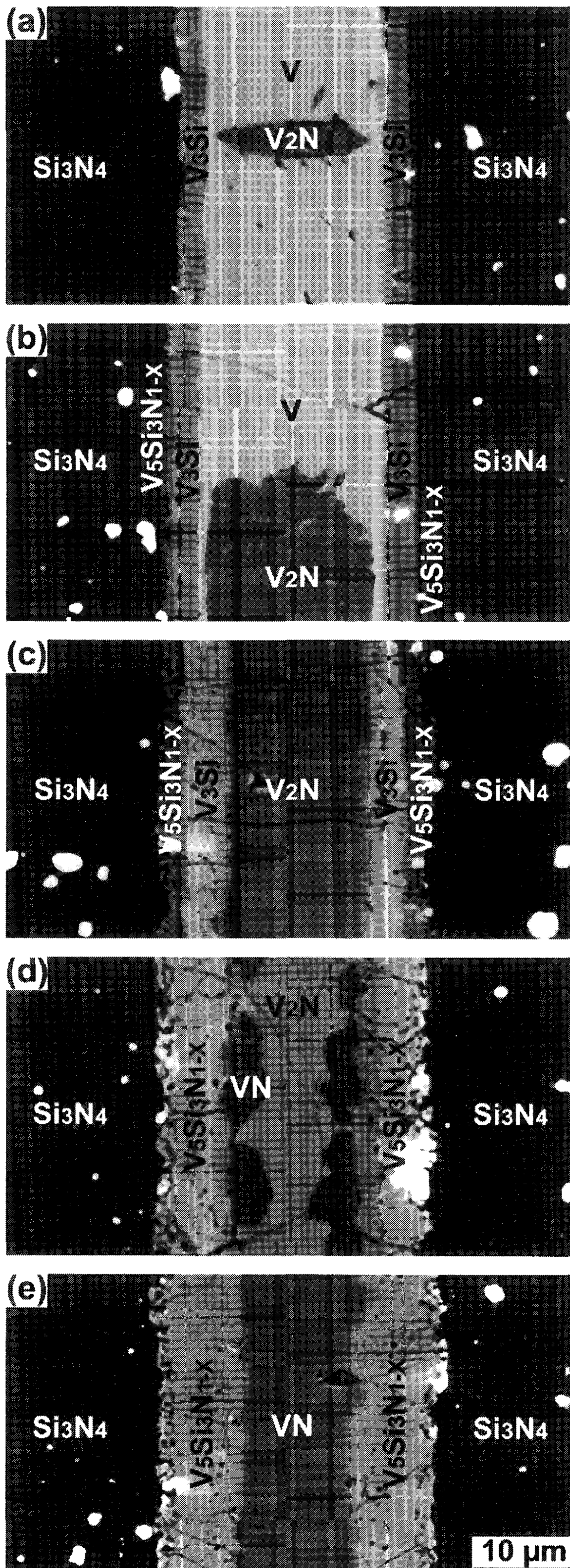

Fig. 4 Five representative stages of the interfacial structure bonded at 1673 K. The bonding time for each joint is (a) 0.9 ks, (b) 1.8 ks, (c) 3.6 ks, (d) 14.4 ks and (e) 32.4 ks, respectively.

The interfacial microstructure formed at 1573 K and above appears different in the early stages of the evolution of the interfacial microstructure from that formed at low-temperatures. **Fig. 4** shows a series of SEM micrographs, which reveal five typical stages of interfacial microstructures bonded at 1673 K for different bonding times, with the result of phase identification. The bonding times for the joints depicted in Figs. 4 (a), (b), (c), (d) and (e) are 0.9 ks, 1.8 ks, 3.6 ks, 14.4 ks and 32.4 ks, respectively. In the first stage shown in Fig. 4(a), a layer of V_3Si adjacent to Si_3N_4 and grains of V_2N inside the V are formed. The difference from the microstructure formed at low-temperatures is that the V_2N grains are not in contact with the V_3Si layer. Thus, the phase sequence observed in this stage is described as Si_3N_4 / V_3Si / V / V+V_2N. The mechanism to prevent the V_2N grains from contacting the V_3Si layer is discussed in the next paragraph. In the second stage shown in Fig. 4(b), a layer of $V_5Si_3N_{1-X}$ is formed between Si_3N_4 and V_3Si. The V_2N grains grow larger but still avoid contact with the V_3Si layer. The phase sequence observed in this stage is described as Si_3N_4 / $V_5Si_3N_{1-X}$ / V_3Si / V / V+V_2N. In the third stage shown in Fig. 4(c), the V is annihilated. The V_2N becomes a layer and finally comes into contact with the V_3Si layer. At this and the later stages, the interfacial microstructure becomes the same as the corresponding stage at low-temperatures, as shown in Figs. 2 (c) and (d). The phase sequence observed in the third and the fourth stages are described as Si_3N_4 / $V_5Si_3N_{1-X}$ / V_3Si / V_2N and Si_3N_4 / $V_5Si_3N_{1-X}$ / V_2N + VN / V_2N, respectively. In the fifth stage shown in Fig. 4(e), the V_2N layer is annihilated. Therefore, only $V_5Si_3N_{1-X}$ and VN remain chemically stable in the final stage. The phase sequence observed at this stage is described as Si_3N_4 / $V_5Si_3N_{1-X}$ / VN.

The V_2N grains do not contact the V_3Si layer in the early stages of high bonding temperatures. The mechanism is deduced from the state of the vanadium lying adjacent to the V_3Si layer. **Fig. 5** shows the detailed composition profile of silicon across the interface bonded at 1673 K for 0.3 ks in comparison with that bonded at 1473 K, 1.8 ks. Both bonding conditions form the V_3Si layer of the same thickness adjacent to Si_3N_4, which

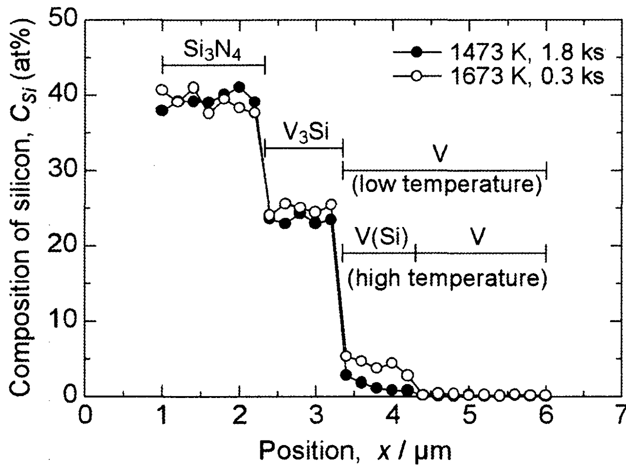

Fig. 5 Comparison of the composition profiles of silicon across the interface of the joints bonded at 1673 K for 0.3 ks and at 1473 K for 1.8 ks.

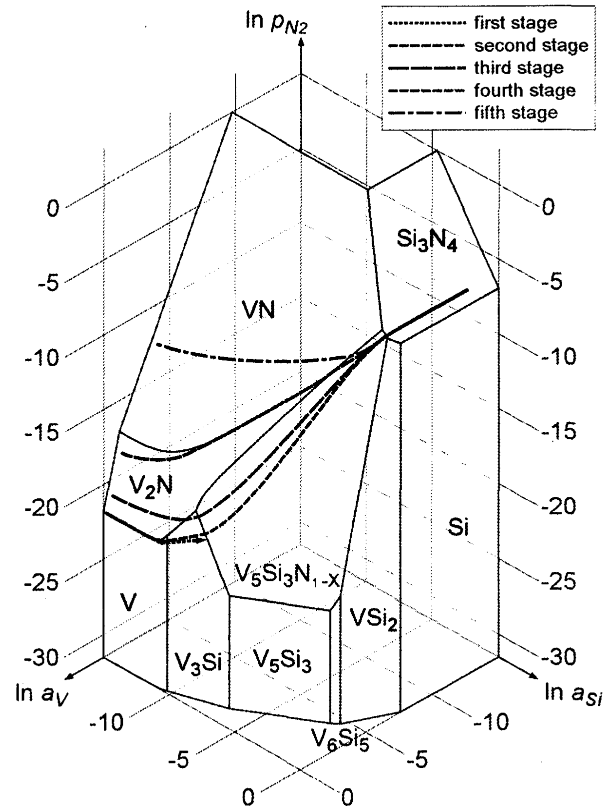

Fig. 6 Chemical potential diagram of the V-Si-N ternary system at 1673 K. The five types of dashed lines depict the phase sequences observed at five different stages of the joint interfaces shown in Fig. 4.

corresponds to the first stage of the evolution in the interfacial microstructure. A 0.8 μm thick zone in the vanadium adjacent to the V_3Si layer containing approximately 4 at% of silicon is detected in the joint bonded at 1673 K. The diffusion zone of silicon in the vanadium, which is named as the V(Si) zone in the following, is not formed at low-temperature conditions, but only at high-temperature conditions. The composition of V-4 at%Si corresponds to the solubility limit of silicon in vanadium at 1673 K[17]. The V-Si-N ternary phase diagram[24] suggests that vanadium saturated with silicon scarcely dissolves nitrogen and cannot coexist with V_2N. Therefore, V_2N is formed inside the vanadium in which silicon is not dissolved. In other words, the V(Si) zone prevents the V_2N grains from contacting the V_3Si layer. Consequently, the phase sequence observed at the first and the second stage at 1673 K should be corrected as Si_3N_4 / V_3Si / V(Si) / V+V_2N and Si_3N_4 / $V_5Si_3N_{1-X}$ / V_3Si / V(Si) / V+V_2N, respectively. This result implies that the interfacial energy of the V_3Si / V is reduced by the formation of the V(Si) zone to a level lower than that of the V_3Si / V_2N. **Fig. 6** shows the V-Si-N ternary chemical potential diagram at 1673 K. The phase sequences observed in Fig. 4, except the metastable first stage, are consistent with the dashed lines drawn on Fig. 6.

The present result in the earliest stage of interfacial reaction showing a V_3Si layer adjacent to Si_3N_4 strongly suggests that the growth of the silicide layers is controlled by diffusion of vanadium instead of silicon through the silicide layers, as depicted in Figs. 2 and 6 with arrows for the phase sequences of the first stages. This conclusion is also derived from the morphology of the V_3Si / V + V_2N interface which is observed in the early stages of low-temperature bonding conditions. The V_3Si layer has two different interfaces on the metal side. One is the interface with the V and the other is that with the V_2N grains. Although two different phases are in contact with the V_3Si layer, the thickness of the layer does not appear different by the difference of the contacting phases. Furthermore, the V_3Si layer grows without embedding V_2N grains at their original positions. This fact indicates that the growth front of the V_3Si layer is not located on the metal side but on the Si_3N_4 side of the layer.

3.3 Growth Behavior of the Reaction Products

In every bonding condition employed in the present study, only V_3Si, $V_5Si_3N_{1-X}$, V_2N and VN are formed at the interfaces. V_3Si and $V_5Si_3N_{1-X}$ appear as layers from their initial state, while V_2N and VN appear as grains initially and then grow to form a layer. In order to estimate the amount of formed grains of V_2N and VN, a representative size of each phase, w_i, was defined as

$$w_i = A_i / 2\, l_i , \qquad (1)$$

where A_i is the observed total area of each phase and l_i is the observed length of the interface. This parameter preserves compatibility with the thickness, the size parameter when each phase achieves the formation of its layer.

The increase and decrease behavior in the thickness of each reaction product interact with each other. **Fig. 7** shows the growth behavior of each reaction product at 1473 K. The representative size and the thickness of each reaction product are plotted as a function of the square root of bonding time, $t^{1/2}$. It is clearly shown that V_3Si,

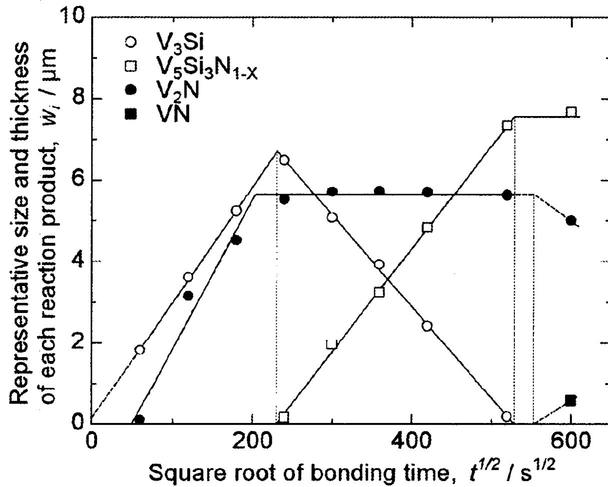

Fig. 7 Growth behavior of each reaction product at 1473 K.

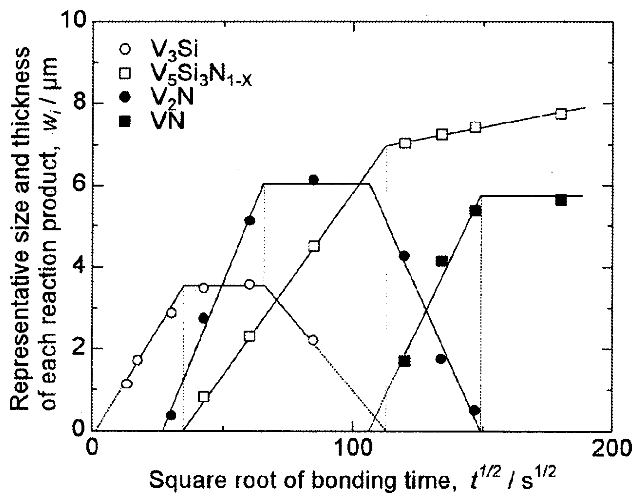

Fig. 8 Growth behavior of each reaction product at 1673 K.

V_2N and $V_5Si_3N_{1-X}$ grow proportionately with the square root of bonding time, obeying the parabolic law, in the initial stage of growth. Only V_3Si appears without showing any latency period. The thickness of the V_3Si layer increases until the $V_5Si_3N_{1-X}$ layer is formed. The formation and growth of the $V_5Si_3N_{1-X}$ layer forces the V_3Si layer to disappear. The growth rate of the $V_5Si_3N_{1-X}$ layer is retained until it comes into contact with the V_2N from the annihilation of the V_3Si layer. Then, the growth is slowed down. The V_2N grains grow until the grains grown from both sides of the foil contact with each other. V_2N keeps its representative size of 5.65 μm until the VN grains are formed. The VN grows reducing the thickness of the V_2N layer. **Fig. 8** shows the growth behavior of each reaction product at 1673 K. Every reaction product grows obeying the parabolic law in its initial stage of growth also at this temperature. The V_3Si layer increases its thickness until the $V_5Si_3N_{1-X}$ layer is formed. In contrast with the behavior at low-temperatures, the layer does not decrease its thickness by the formation of the $V_5Si_3N_{1-X}$ layer, keeping its thickness of 3.55 μm until the V_3Si layer contacts the V_2N layer. The formation of the

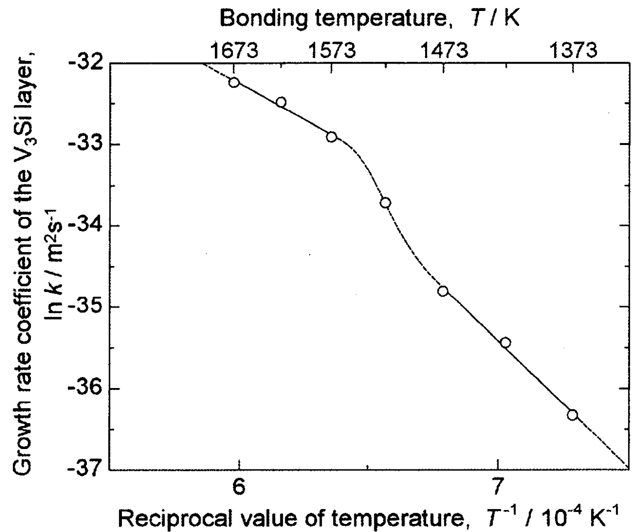

Fig. 9 Arrhenius plot of the growth rate coefficient of the V_3Si layer.

V_3Si / V_2N interface, which indicates the annihilation of the V phase, also stops the parabolic growth of the V_2N. The V_2N layer maintains its thickness of 6.04 μm until the VN grains are formed. The annihilation of the V_3Si layer results in the suppression of the growth of the $V_5Si_3N_{1-X}$ layer. On the other hand, the annihilation of the V_2N layer stops the growth of the VN. The interaction of the growth behavior of each reaction product is summarized as follows: the V_3Si layer stops its parabolic growth when the $V_5Si_3N_{1-X}$ layer is formed. The reduction in its thickness starts when it contacts with the V_2N. The $V_5Si_3N_{1-X}$ layer slows down its growth by contacting the V_2N, which corresponds to the annihilation of the V_3Si layer. The V_2N stops its parabolic growth when coming into contact with the V_3Si layer and the contacting of the grains grown from both sides are achieved. The reduction in its representative size starts by the formation of the VN grains. The VN stops its parabolic growth when the V_2N is annihilated.

The change in the thickness of the V_3Si layer is observed to be sensitively affected by the behavior of the V_2N phase. As discussed in the last section, whether the V_2N contacts with the V_3Si layer is determined by the formation of a thin V(Si) zone at the V_3Si / V interface. Since silicon can diffuse into vanadium from the beginning of the bonding treatment at high-temperature conditions, the V(Si) zone can affect the growth behavior of the V_3Si layer even in the initial stage of parabolic growth. **Fig. 9** shows the dependence of the growth rate coefficient of the V_3Si layer, k, on the bonding temperature regarding the Arrhenius-type function

$$\ln k = \ln k_0 - Q / RT, \qquad (2)$$

where k_0 is the pre-exponential factor for the growth rate of the V_3Si layer, Q is the apparent activation energy for the growth of the V_3Si layer, R is the gas constant and T is the bonding temperature. The dependence of the

Table 2 A list of the pre-exponential factors of the growth rate and the apparent activation energies for the growth of the V_3Si layer at each temperature range.

Temperature range, T / K	Pre-exponential factor for the growth rate, k_0 / m^2s^{-1}	Apparent activation energy for the growth, Q / kJ mol^{-1}
1373 - 1473	1.30×10^{-6}	260
1573 - 1673	3.66×10^{-10}	146

growth rate on the bonding temperature for the low-temperature bonding condition appears with different line from that for the high-temperature bonding condition, revealing a transition-temperature range between 1473 K and 1573 K. The interfacial microstructure of the joints bonded at the temperatures in this range shows that the V_2N grains are formed without contacting the V_3Si layer even at 1498 K. This result indicates that the V(Si) zone starts its formation at the onset temperature of the transition observed in Fig. 9. The values of k_0 and Q for the low- and the high-temperature bonding condition calculated from Fig. 9 are listed in **Table 2**. The activation energy for the growth of the V_3Si layer at the high-temperature bonding condition appears lower than that at the low-temperature bonding condition. This result suggests that the formation of the V(Si) zone adjacent to V_3Si reduces the activation energy of the growth of the V_3Si layer. As discussed in the previous section, the growth of the V_3Si layer is controlled by the diffusion of vanadium through the layer, and the V(Si) zone reduces the interfacial energy of the V_3Si / V phase boundary to a level lower than that of the V_3Si / V_2N. These results support the view that the V(Si) zone improves the diffusion of vanadium in the V_3Si layer by reducing the activation energy for dissolution of vanadium into V_3Si. Therefore, the apparent activation energy for the growth of the V_3Si layer corresponds to that for the dissolution of vanadium into the V_3Si layer.

Figs. 7 and 8 indicate that the V_3Si layer grows up to 6.70 μm before the $V_5Si_3N_{1-X}$ layer is formed at the bonding temperature of 1473 K and up to 3.55 μm at 1673 K. This result indicates that the Si_3N_4 / V_3Si interface is more stable at lower temperatures. Since the Si_3N_4 / V_3Si interface is thermodynamically metastable, sufficient amounts of vanadium are supplied to the interface to form V_3Si adjacent to Si_3N_4 in the first stage of interfacial reaction. Therefore, the formation of the $V_5Si_3N_{1-X}$ layer starts when the diffusion flux of vanadium in the V_3Si layer is reduced below a certain level by increasing the thickness of the V_3Si layer. The diffusion flux of vanadium through the V_3Si layer, J_V, is determined according to the Fick's first law:

$$J_V = -D_V\,(\partial C_V / \partial x), \tag{3}$$

where D_V and $\partial C_V/\partial x$ are the diffusion coefficient of vanadium through V_3Si and the spatial composition gradient of vanadium in the V_3Si layer, respectively. As shown in Fig. 1(b), however, the composition of vanadium in the V_3Si layer is almost uniform. Thus, the diffusion cannot be driven by the composition gradient. Since the diffusion of an element is caused by the gradient of the chemical potential, to replace the composition, C_V, with the activity of vanadium, a_V, will explain the diffusion more correctly. Thus, the equation (3) can be modified as

$$J_V = -D_V\frac{\partial a_V}{\partial x} = -D_V\frac{\partial \exp(\mu_V/RT)}{\partial x} = -\frac{D_V}{RT}\exp\left(\frac{\mu_V}{RT}\right)\frac{\partial \mu_V}{\partial x} \tag{4}$$

in the isothermal condition, where μ_V is the chemical potential of vanadium. Equation (4) indicates that the diffusion flux depends proportionately on the spatial gradient of the chemical potential of vanadium, $\partial\mu_V/\partial x$. The value of $\partial\mu_V/\partial x$ was roughly estimated by dividing the difference in the chemical potential of vanadium at the Si_3N_4 / V_3Si and the V_3Si / V+V_2N interfaces, $\Delta\mu_V$, with the observed critical thickness of the V_3Si layer for the formation of the $V_5Si_3N_{1-X}$ layer, w_{V3Si}*. The calculation of $\Delta\mu_V/w_{V3Si}$* for the bonding temperatures of 1473 K and 1673 K yields -3.36×10^9 and -3.31×10^9 J mol^{-1} m^{-1}, respectively. Both values appears almost the same. This result suggests that the $V_5Si_3N_{1-X}$ layer is formed to establish a local equilibrium at the interface with Si_3N_4 when the spatial gradient of the chemical potential of vanadium in the V_3Si layer decreases to a value below -3.3×10^9 J mol^{-1} m^{-1}, being independent of the bonding temperature, by increasing the thickness of the V_3Si layer.

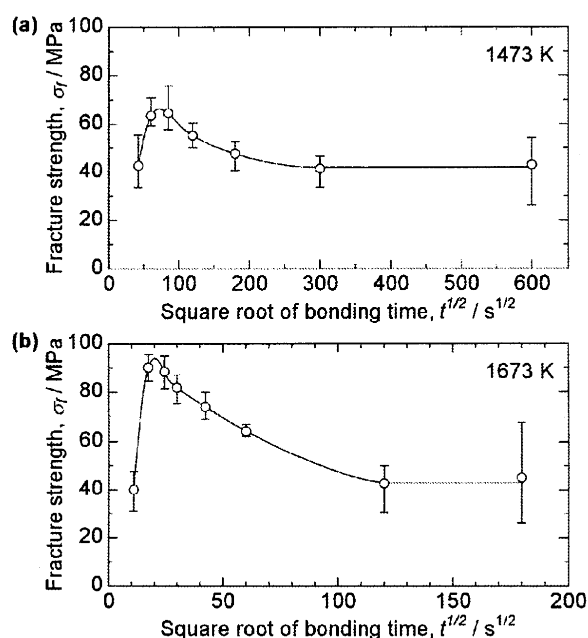

Fig. 10 Dependence of the fracture strength of the Si_3N_4 / V joints on the bonding time. (a) bonded at 1473 K, (b) at 1673 K.

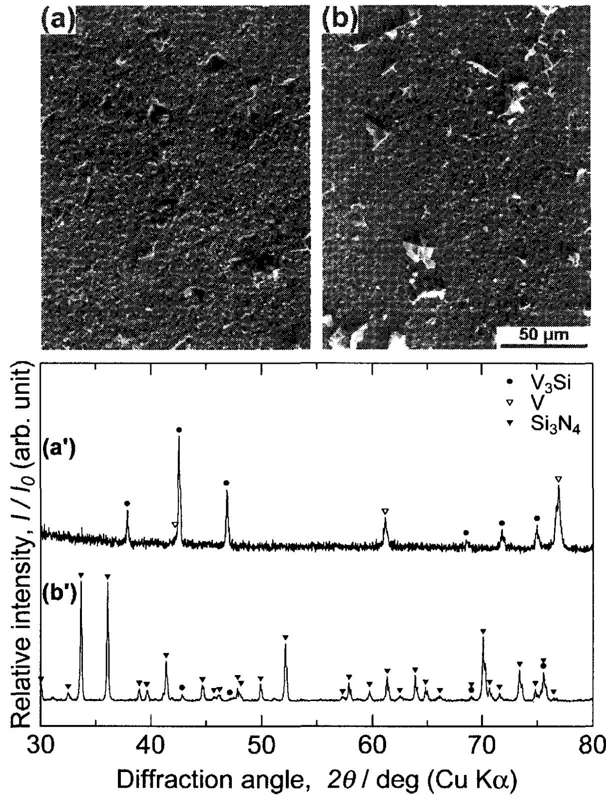

Fig. 11 SEM micrographs and corresponding XRD patterns taken from both sides of the fracture surfaces of a joint bonded at 1473 K for 3.6 ks. (a) and (a') were taken from the V side, (b) and (b') from the Si_3N_4 side.

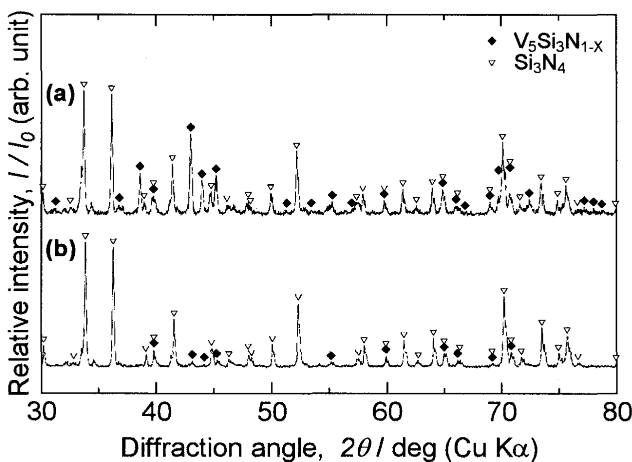

Fig. 12 XRD patterns taken from both sides of the fracture surfaces of a joint bonded at 1473 K for 360.0 ks. (a) were taken from the V side, (b) from the Si_3N_4 side.

3.4 Joint Strength and Fracture

The fracture strength of the joints changes depending on the bonding time. **Figs. 10** (a) and (b) depict the dependence of the fracture strength on the bonding time for the joints bonded at 1473 K and 1673 K, respectively. The fracture strength of the joints bonded at 1473 K improves up to a bonding time of 5.2 ks, at which the maximum average-strength of 67 MPa is obtained.

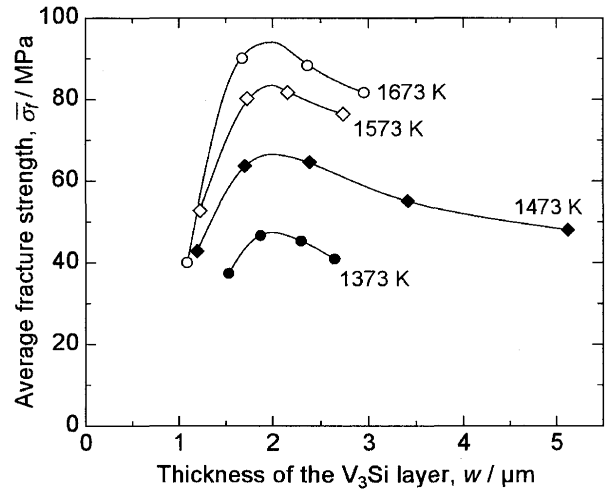

Fig. 13 Relation between the average fracture strength and the thickness of the V_3Si layer.

Referring to Fig. 7, the bonding condition of 1473 K for 5.2 ks corresponds to the formation of a 2.0 μm-thick V_3Si layer adjacent to Si_3N_4. A prolonged bonding time over 5.2 ks gradually reduces the fracture strength down to 42 MPa. The fracture strength of the joints bonded at 1673 K increases up to a bonding time of 0.4 ks, at which the maximum average-strength of 94 MPa is obtained. The bonding condition of 1673 K for 0.4 ks corresponds to the formation of a 2.0 μm-thick V_3Si layer adjacent to Si_3N_4. The prolonged bonding time over 0.4 ks gradually reduces the fracture strength down to 43 MPa and significantly expands the scatter in the data.

Fig. 11 shows a pair of SEM micrographs and corresponding XRD patterns taken from both sides of the fracture surfaces of a joint bonded at 1473 K for 3.6 ks, at which a strong joint of 64 MPa was obtained. Both fracture surfaces appear microscopically flat, indicating that the fracture occurs at the interface in a brittle mode. The side on which the vanadium foil is remaining is named the "V side", while the other side is named as the "Si_3N_4 side". On the V-side surface (Fig. 11(a)), only V_3Si is detected, in which pits are dispersed. The XRD pattern taken from the V side (Fig. 11(a')), in which only V_3Si and V are detected, agrees with this analysis result. Corresponding to the pits on the V-side surface, sharp-edged particles of V_3Si are observed on the Si_3N_4-side surface (Fig. 11(b)). In agreement with the EPMA, the XRD pattern taken from the Si_3N_4 side (Fig. 11(b')) indicates that Si_3N_4 and small amounts of V_3Si on the surface. Based on these results, the fracture is determined to occur mainly at the Si_3N_4 / V_3Si interface and partly inside the V_3Si layer. **Fig. 12** shows a pair of XRD patterns taken from a joint bonded at 1473 K for 360.0 ks, at which the joint strength is reduced to 43 MPa. The XRD pattern taken from the V side (Fig. 12(a)) indicates the existence of Si_3N_4 and $V_5Si_3N_{1-X}$ on the surface. However, Si_3N_4 is observed only at the areas where the insert foil has been chipped off. Thus, the peaks of Si_3N_4 in the pattern have originated from the counterpart of the

joint. On the other hand, Si_3N_4 and $V_5Si_3N_{1-X}$ are detected in the XRD pattern taken from the Si_3N_4 side (Fig. 12(b)). Therefore, the fracture is determined to occur at the $V_5Si_3N_{1-X}$ in the vicinity of the Si_3N_4 / $V_5Si_3N_{1-X}$ interface. The analysis of the fractured surfaces of the joints bonded at 1673 K results in the same conclusion as that of 1473 K: the high-strength joints are fractured at the Si_3N_4 / V_3Si interface and the joints bonded with the prolonged bonding time are fractured at the $V_5Si_3N_{1-X}$ in the vicinity of the Si_3N_4 / $V_5Si_3N_{1-X}$ interface.

The maximum fracture strength is achieved when the thickness of the V_3Si layer is 2.0 μm. Ito *et al.*[15], also, have reported the formation of a 2 μm-thick V_3Si layer adjacent to Si_3N_4 at the optimum bonding condition. **Fig. 13** shows the relation between the average fracture strength and the thickness of the V_3Si layer. At every bonding temperature between 1373 K and 1673 K, the maximum fracture strength is obtained when the thickness of the V_3Si layer is 2.0 μm, regardless of the bonding temperature. In addition, a higher bonding temperature leads to a higher maximum fracture strength. The improvement and deterioration behavior of the fracture strength without the formation of the $V_5Si_3N_{1-X}$ layer is considered to result from the competition process of the following two factors. One is the improvement in the fracture strength, explained by the chemical-bond formation process on the atomic scale at the Si_3N_4 / V contact area and by the plastic deformation of the vanadium foil to expand the contact area. Since the yield strength of vanadium is lower at higher temperatures, the fraction of contact area on the atomic scale becomes larger at higher temperatures to increase the maximum fracture strength. The other factor is the deterioration of the fracture strength, explained by the magnitude of the thermal residual stress as a function of the thickness of the V_3Si layer, especially that concentrated at the edge of the bond interface. Although the mismatch of the thermal expansion coefficient for the Si_3N_4 / V_3Si interface is reported[14], the yield strength and the elastic modulus of V_3Si as functions of the temperature are not found in the literature, but are necessary for the estimation of the magnitude of the thermal residual stress.

The $V_5Si_3N_{1-X}$ layer is formed at the interface of the joints bonded a the prolonged bonding time. The average fracture strength of such joints converges to a value of approximately 42 MPa, being insensitive to the bonding temperature. The fracture of such joints occurs at the $V_5Si_3N_{1-X}$ in the vicinity of the Si_3N_4 / $V_5Si_3N_{1-X}$ interface, which corresponds to the position where the segregation of large-sized voids is observed as shown in Figs. 2 and 4. Therefore, the fracture is considered to occur by crack propagation connecting these voids. Since the voids are formed by N_2 gas generated during cooling, the fracture property of the joints at this state of interfacial microstructure is sensitive to the behavior of nitrogen. For example, regarding to Figs. 7, 8 and 10, the scatter of the fracture strength increases when the $V_5Si_3N_{1-X}$ contacts with the V_2N. This change in the microstructure will affect the formation and segregation behavior of the voids.

4. Summary

Si_3N_4 was bonded to vanadium foils by solid state diffusion bonding. The interfacial microstructure and reaction kinetics were analyzed in detail by means of SEM, EPMA and XRD. The strength of the joints was estimated by a shear fracture test. The following points were established.

1) The interfacial phase sequence of the Si_3N_4 / V joints bonded at 1473 K and below reveals four stages of transition as follows: (i) Si_3N_4 / V_3Si / $V+V_2N$ / V, (ii) Si_3N_4 / $V_5Si_3N_{1-X}$ / V_3Si / $V+V_2N$, (iii) Si_3N_4 / $V_5Si_3N_{1-X}$ / V_3Si / V_2N, and (iv) Si_3N_4 / $V_5Si_3N_{1-X}$ / V_2N + VN / V_2N. At the bonding temperatures of 1498 K and higher, the V_2N grains are prevented from contacting the V_3Si layer by the V(Si) zone. At these temperatures, five stages of transition in the interfacial phase sequence are observed as follows: (i) Si_3N_4 / V_3Si / V(Si) / $V+V_2N$, (ii) Si_3N_4 / $V_5Si_3N_{1-X}$ / V_3Si / V(Si) / $V+V_2N$, (iii) Si_3N_4 / $V_5Si_3N_{1-X}$ / V_3Si / V_2N, (iv) Si_3N_4 / $V_5Si_3N_{1-X}$ / V_2N + VN / V_2N, and (v) Si_3N_4 / $V_5Si_3N_{1-X}$ / VN. The Si_3N_4 / V_3Si interface observed in the first stage is metastable. These phase sequences, except the metastable interface, are successfully expressed on the proposed chemical potential diagram.
2) The growth front of the V_3Si layer is located on the Si_3N_4 side, indicating that the diffusion of vanadium through the V_3Si layer dominates the growth of the layer.
3) The increase and decrease behavior in the thickness of each reaction product interacts with each other. Every reaction product grows obeying the parabolic law in its initial stage of growth. The pre-exponential growth constant and the activation energy for the growth of the V_3Si layer appear different between the high- and low-temperature bonding conditions. The formation of the $V_5Si_3N_{1-X}$ layer starts when the spatial gradient of the chemical potential of vanadium in the V_3Si layer decreases to a value below -3.3×10^{9} J mol^{-1} m^{-1} by the growth of the V_3Si layer.
4) The maximum fracture strength is achieved when the thickness of the V_3Si layer is 2.0 μm. A higher bonding temperature leads to a higher maximum fracture strength. The fracture of the joints bonded at this condition occurs in a brittle mode mainly at the Si_3N_4 / V_3Si interface and partly inside the V_3Si layer. A prolonged bonding time gradually reduces the fracture strength down to 42 MPa. The joints are fractured at the $V_5Si_3N_{1-X}$ in the vicinity of the Si_3N_4 / $V_5Si_3N_{1-X}$ interface by crack propagation connecting the voids.

Acknowledgement

The authors express their gratitude to Dr. Harumi Yokokawa, National Institute of Materials and Chemistry, for the discussion on the reaction phenomena between ceramics and metals from thermodynamical point of

view.

REFERENCES

1) F. L. Riley: *ENCYCLOPEDIA OF MATERIALS SCIENCE AND ENGINEERING*, ed. by M. B. Bever, Pergamon Press, London, 1986, Vol. 6, pp. 4412-4415.
2) F.W. Clinard, Jr., G.F. Hurley and R.W. Klaffky: Res Mechanica **8** (1983) 207-234.
3) R.F. Mattas and M.C. Billone: J. Nucl. Mater. **233-237** (1996) 72-81.
4) D.L. Smith, M.C. Billone, S. Majumdar, R.F. Mattas and D.-K. Sze: J. Nucl. Mater. **258-263** (1998) 65-73.
5) D.L. Smith, M.C. Billone and K. Natesan: Int. J. Refractory Met. & Hard Mater. **18** (2000) 213-224.
6) D.L. Smith, J.-H. Park, I. Lyublinski, V. Evtikhin, A. Perujo, H. Glassbrenner, T. Terai and S. Zinkle: Fusion Eng. and Design **61-62** (2002) 629-641.
7) Y. Nemoto, K. Ueda, M. Satou, A. Hasegawa and K. Abe: J. Nucl. Mater. **258-263** (1998) 1517-1522.
8) R. Yasuda, M. Satou, A. Hasegawa and K. Abe: J. Nucl. Mater. **258-263** (1998) 1528-1532.
9) H. Mori, T. Sakata, H. Yasuda and M. Maeda: J. Vac. Sci. Tech. B **12** (1994) 2376-2379.
10) Y. Nakao, K. Nishimoto and K. Saida: Trans. Jpn. Weld. Soc. **20** (1989) 66-76.
11) Y. Morizono, T. Nakata, M. Nishida and A. Chiba: J. Ceram. Soc. Jpn. **103** (1995) 810-815, in Japanese.
12) S.D. Peteves, M. Paulasto, G. Ceccone and V. Stamos: Acta Mater. **46** (1998) 2407-2414.
13) P. Lamparter, S. Steeb and A. Gukelberger: High Temperatures – High Pressures **3** (1971) 727-740.
14) J. C. Schuster, F. Weitzer, J. Bauer and H. Nowotny: Mater. Sci. Eng. **A105/106** (1988) 201-206.
15) Y. Ito, K. Kitamura and M. Kanno: J. Mater. Sci. **28** (1993) 5014-5018.
16) I. Gotman and E.Y. Gutmanas: Acta Metall. Mater. **40** (1992) Suppl. S121-S131.
17) *Binary Alloy Phase Diagrams*, ed. by T.B. Massalski, American Society for Metals, Metals Park, Ohio, 1986, pp. 2060-2062.
18) *Binary Alloy Phase Diagrams*, ed. by T.B. Massalski, American Society for Metals, Metals Park, Ohio, 1986, pp. 1656-1659.
19) *Powder Diffraction File*, JCPDS, 33-1160.
20) *Powder Diffraction File*, JCPDS, 19-1405.
21) *Powder Diffraction File*, JCPDS, 32-1413.
22) *Powder Diffraction File*, JCPDS, 22-1058.
23) *Powder Diffraction File*, JCPDS, 40-956.
24) R. Andruszkiewicz and R. Horyń: J. Less-Common Met. **124** (1986) 205-210.
25) *Phase Diagrams of Ternary Boron Nitride and Silicon Nitride Systems*, ed. by P. Rogl and J.C. Schuster, ASM International, Materials Park, Ohio, 1992, pp. 205-207.